Journal of Catalysis **184,** 224–235 (1999)
Article ID jcat.1999.2427, available online at http://www.idealibrary.com on IDEAL®

Dynamic Isotope Tracing: Role of Subsurface Oxygen in Ethylene Epoxidation on Silver

Christopher J. Bertole and Charles A. Mims[1]

Department of Chemical Engineering and Applied Chemistry, 200 College Street, University of Toronto, Toronto, Ontario, Canada M5S3E5

Received October 22, 1998; revised January 22, 1999; accepted January 22, 1999

We have used isotope transients, $^{16}O_2$–$^{18}O_2$, at reaction steady state to investigate the epoxidation of ethylene over unsupported silver powder catalysts. The reactive oxygen inventory at steady state consists of two types: one with a short residence time (<1s on the catalyst) and another with a long residence time (>15s). The latter (assigned to subsurface oxygen) can comprise as much as 2.5 monolayer-equivalents. Ethylene oxide selectivity correlates strongly with the availability of the subsurface oxygen. This correlation holds for both chlorine-free and chlorine-inhibited catalysts and over a range of temperatures. © 1999 Academic Press

Key Words: **ethene; epoxidation; silver; chlorine; isotope transients; subsurface oxygen; kinetics; selectivity.**

INTRODUCTION

The mechanism of ethylene epoxidation over silver has been the subject of intense scrutiny and debate (1–4). Different types of oxygen exist on silver, depending on adsorption conditions; these include molecular, subsurface, and various forms of surface atomic oxygen (1–4). Their roles in ethylene epoxidation are critical, and much work has focused on this aspect. Solid experimental evidence now exists supporting epoxidation by a monatomic oxygen intermediate (5–9). Grant *et al.* [6] proposed that the effective charge state on surface atomic oxygen determines product selectivity. Adsorbed oxygen with electrophilic character attacks the electron rich ethylene double bond to form ethylene oxide, while adsorbed oxygen with nucleophilic character forms total oxidation products (4).

Subsurface oxygen is important for ethylene epoxidation (3, 5). It exchanges reversibly with the surface (10–13) and appears in both reaction products (9). Furthermore, it has been proposed that subsurface oxygen changes the surface binding of oxygen, making it more susceptible to epoxidation (6). An increased inventory of oxygen, both surface and subsurface, may increase the electrophilicity of the oxygen adlayer. The mechanism of chlorine promotion is also not fully understood, although many ideas have surfaced (1, 5, 14–16). Coadsorbed chlorine increases the amount of subsurface oxygen which appears during temperature programmed desorption (TPD) experiments (14–17). This implies that the transport rate of oxygen from the bulk is increased; however, it is not known whether the same effect occurs under steady state reaction conditions. The increased oxygen diffusion rates may promote the formation of electrophilic-type oxygen at defect sites (18). Chlorine may also draw electron density away from oxygen atoms, making them more electrophilic (6), a role also attributed to subsurface oxygen.

Dynamic isotope tracing is a powerful technique to obtain information about the number and amounts of surface intermediates, their surface lifetimes, and the sequence of reaction steps without disturbing steady state reaction conditions (19–21). It involves monitoring the time-resolved appearance of isotopically labelled atoms from reactants as they become incorporated into reaction products. The aim of this study is to use dynamic isotope tracing to obtain information about the active oxygen pools on unsupported silver powder catalysts during steady state ethylene epoxidation and observe the effects of chlorine on their reactivity and quantity. In particular, the following switch was made at reaction steady state:

$$[C_2H_4 : {}^{16}O_2 : \mathrm{Ar/Ne}](1) \rightarrow [C_2H_4 + {}^{18}O_2 + \mathrm{Ar}](2).$$

The "washout" of catalyst bound ^{16}O into both reaction products (and into molecular oxygen) reveals the amounts of oxygen involved in the steady state mechanism and their residence time on the catalyst. Two previous limited studies of ethylene oxidation on silver by such experiments have been reported (22, 23).

The pathway by which oxygen appears in the products can be obscured by scrambling the oxygen in the newly formed products with the catalyst and (via the catalyst) with the other gas phase molecules. The "washout" data in the above experiments are affected by such processes, which are generally facile over oxide catalysts (19, 24, 25), even for formaldehyde and other "fragile" molecules. On silver, carbon dioxide rapidly scrambles oxygen with surface-bound

[1] To whom correspondence should be addressed.

0021-9517/99 $30.00

oxygen species under non-steady state conditions (7, 26–28), and ethylene oxide has been reported to scramble its oxygen with a calcium promoted silver catalyst at 100°C under non-steady state conditions (26). Therefore, we include measurements of the oxygen exchange behaviour at the conditions of this study to aid in the interpretation of the isotope transients results. In addition, isotope infusion via such exchange reactions is used to probe the oxygen pools at a point in the mechanism which differs from that of molecular oxygen. Specifically, we perform experiments where product molecules with a different isotopic label from the molecular oxygen are included in the feed: i.e., $[C^{18}O_2 + {}^{16}O_2 + C_2H_4]$ and $[{}^{18}O_2 + C_2H_4 + C_2H_4{}^{16}O]$. The appearance of the oxygen from the product molecule in the other product, or in bimolecular oxygen, is then monitored, including the time response to a sudden introduction of isotope in this manner. Water scrambles oxygen as well (26, 28), but these exchange reactions were not performed in the present study.

EXPERIMENTAL

Materials and Apparatus

Reactor. The reactor system is similar to those described previously (29). Briefly, reactions were performed in a single pass, differential, down-flow, tubular (4 mm id) quartz, fixed bed reactor. The catalyst charge was supported on a quartz wool plug in the reactor tube. The reaction temperature was monitored by a type K thermocouple in a quartz sheath (1 mm OD) in contact with the top of the catalyst bed. The reactor effluent was analyzed by GC (Hewlett Packard HP5880A) and by MS (UTI 100C) through a differentially pumped quartz capillary leak placed directly below the catalyst bed. A similar leak after the GC column allowed GC-MS analysis of trapped aliquots of gas. This latter capability provides clean isotopic analysis of gas mixtures with difficult overlaps in the fragmentation patterns of the components. A PC-based computer program controls the collection of time-resolved mass spectrometric data.

Catalysts. Silver powder catalysts were made from three different batches from Aldrich: (a) 99.99% pure (trace impurities given as 8 ppm Si, 6 ppm Fe, 3 ppm Zn, and 0.6 ppm Mg); (b) 99.999% pure (trace impurities were 4 ppm Pb, 2 ppm Hg, 1 ppm Fe, 1 ppm Na, 0.7 ppm Ca, 0.3 ppm Cu, 0.3 ppm Zn, and 0.1 ppm Mg); and (c) also 99.999% (9 ppm Ca, 3 ppm Fe, 2 ppm Zn, and 1 ppm Mg). The surface areas of the as-received powders were 0.11 m^2/g (single point N_2 BET); this value agrees with typical reported surface areas for silver powder (30–32). The post-reaction samples were too small for reliable BET measurements and we resorted to primary particle size analysis from SEM photographs to estimate the surface areas. Where necessary to reduce the pressure drop in the reactor, the as-received catalyst powders were pressed into 13-mm diameter pellets using a die press to 15,000 psi. Pellets were then crushed and sieved to a particle size of 50–100 mesh (0.15–0.30 mm).

XPS was used to determine surface impurity and chlorine concentrations. The XP spectra were obtained on a Leybold–Heraeus EA-11 electron energy spectrometer at a constant pass energy of 200 eV and with unmonochromatized Al $K\alpha$ X rays. The Cl/Ag atomic ratios in the near surface region were obtained by comparing the Cl $2p_{3/2,1/2}$ intensity to the Ag $3d_{5/2,5/2}$ intensity (including shakeup features), both normalized to their reported sensitivity factors (33).

Gases. The purchased reactor gases used in these experiments were $^{16}O_2$ (Matheson, 99.98%), C_2H_4 (Matheson, 99.9%), $C^{18}O_2$ (ICON, 5% CO_2 at 99 at.% ^{18}O, balance Ar), $C^{18}O_2$ (Isotec, 97.7 at.% ^{18}O), $C_2H_4{}^{16}O$ (Scott S.G., 2% C_2H_4O, balance N_2), and Ar (Matheson, 99.999%). All gases were used without further purification. Custom gas mixtures were made for various experiments by filling lecture bottles with the desired components on a stainless steel vacuum line. Chlorine treatment of the catalysts was accomplished using a custom mix of ethylene and 1,2-dichloroethane (Caledon, 99.0%). This mixture was prepared by serial dilution by ethylene of gas from another bottle of ethylene (20 atm total pressure) saturated with 1,2-dichloroethane vapour at room temperature. The total concentration of 1,2-dichloroethane in this gas was calculated to be approximately 10 ppm. Chlorine dosing procedures are described in the Procedures section.

Procedures

Experimental conditions. Table 1 lists the conditions and catalyst histories for each of the isotope transient experiments. The different pretreatments and conditions produced catalysts with a wide variety of reactivities and selectivities. Each fresh catalyst sample is represented by a separate number and each data set involving that catalyst by a subcharacter. Experiments inclusive to each data set were carried out in succession; the data sets for each batch of catalysts were performed in sequence without going offline.

A typical reaction sequence before the isotope transient involved a selected catalyst pretreatment (Cl dose and other conditioning), followed by a run-in period at the selected condition, and finally a short kinetic characterization (indicated by K in Table 1). These kinetics characterizations occasionally (1a, 1b) involved measuring the reaction orders, at other times only activity maintenance and selectivity at standard conditions ($C_2H_4 : O_2 : \text{Inert} = 1 : 1 : 4$, total pressure = 110 kPa). The isotopically labelled gas flow was then established and the isotope switch performed. The reaction sets 1a and 1b, performed sequentially on the same

TABLE 1

Summary of Experimental Conditions for Isotopic Transients

Experiment number[a]	Temperature/ °C	Gas flow/ $cm^3\ min^{-1}$ [b]	Ag mass/g	Prior to isotopic transient		After isotopic transient		
				Chlorine dose[c]	Summary of catalyst exposure[d]	CO_2 exchange	EO exchange	XPS
1a	227	18	0.46	N	1h/227°C + K(1h)	Y	N	N
1b	225	18	—	Y	**1a** + Cl (10cc) + 1h/225°C + K(1h)	Y	N	Y
2a	187	18	0.50	N	24h/187°C + K(1h)	Y	Y	N
2b	221	18	—	N	**2a** + 1h/221°C + K(1h)	Y	Y	Y
3a	243	18	—	Y	Cl (3/4h/252°C) + 1h/243°C + K(1h)	Y	N	N
3b	266	18	—	Y	**3a** + 2h/266°C + K(1)	Y	N	Y
4	285	18	0.50	N	redox[e] 72h/390°C + 1400h/285°C + K(1h)	Y	Y	Y
5	288	30	0.48	N[f]	24h/288°C + K(1h)	Y	Y	Y

[a] Experiment number indicates catalyst batch, letter indicates the experiment (in sequence) with that catalyst.
[b] Total gas flow rates at standard conditions (110 kPa, 298°K) ($C_2H_4 : O_2 : Inert = 1:1:4$, total pressure = 110 kPa).
[c] Chlorine doses are described in the text.
[d] Time at temperature in the standard feed gas composition; *K*, kinetic characterization (times indicated—various gas mixtures).
[e] Redox cycles described in text.
[f] This catalyst had chlorine on the surface—see text.

catalyst with an intervening chlorine dose, provide the most direct comparison of the effect of chlorine. Reaction sets 2 and 3 studied temperature dependence of chlorine-free and chlorine-dosed catalysts, respectively. Catalyst 4 was subjected to 12 sequential redox cycles at 390°C. Each cycle consisted of 3 h in a 10 cm^3/min flow of 20% O_2 (balance Ar) followed by 3 h in 16 cc/min of 60% H_2, balance Ar). This treatment, similar to that recommended in Ref. (30) to obtain reproducible oxygen uptakes, substantially reduced the reactivity of the catalyst. Experiment 5 is a high temperature run without the catalyst conditioning in 4.

Chlorine. The chlorine dose for catalyst 1 was administered by syringe injection of 10 cm^3 of the ethylene–1,2-dichloroethane (10 ppm) mixture slowly into the reactant stream. For catalyst 3, the chlorine was administered by a 40-min exposure to the reactant mixture containing approximately 10 ppm dichloroethane (mixed in the ethylene). These chlorine doses reduced the catalyst activity while increasing the selectivity in all cases. These changes to the catalyst were stable for the duration of the rest of the experiments on that particular catalyst. Although catalyst 5 was not deliberately exposed to chlorine, it was undoubtedly exposed to residual chlorine left in the flow system contaminated by a high partial pressure of 1,2-dichloroethane.

Isotopic transients. The isotope switches were performed after the two feed stream ($C_2H_4 : {}^{16}O_2$, Ar(Ne) over the catalyst, $C_2H_4 : {}^{18}O_2$, Ar in the bypass) flows were stabilized and the pressures precisely balanced. All were done with the standard gas composition ($C_2H_4 : O_2 : Inert = 1:1:4$); the inert component of the $^{16}O_2$ stream contained 7% Ne tracer to mark the washout of the reactor gas volume. Both the forward and reverse transient (return to unlabelled reactant) were recorded; the reverse transient initiated after the ^{16}O content in the products had decreased to less than 5%. The isotopic composition was monitored by recording $m/e = 22$ (Ne^+), 29 ($HC^{16}O^+$, the major peak of $C_2H_4{}^{16}O$ and $^{13}C^{12}CH_4^+$ from ethylene), 31 ($HC^{18}O^+$, major peak of $C_2H_4{}^{18}O$, no interferences), 32 ($^{16}O_2^+$), 34 ($^{16}O^{18}O^+$), 36 ($^{18}O_2^+$), 44 ($C^{16}O_2^+$, $C_2H_4{}^{16}O^+$-20% of $HC^{16}O^+$, $C_2H_2{}^{18}O^+$ (7% of $HC^{18}O^+$), 46 ($C_2H_4{}^{18}O^+$-20% of $HC^{16}O^+$), and 48 ($C^{18}O_2^+$) intensities. The composition obtained by mass spectrometry was checked by GCMS analysis of aliquots captured during a repeat of the experiment. This procedure provided a check for the presence of mass spectrometer artifacts such as scrambling between oxygen and the products in the mass spectrometer.

Oxygen scrambling. Exchange between $C^{18}O_2$ and the catalyst was investigated by adding a small flow of $C^{18}O_2$ into the $^{16}O_2$ containing standard reactant mixture and monitoring the effluent for ^{18}O in ethylene oxide, oxygen, and carbon dioxide. A control experiment with the empty reactor was also performed to ensure no reactor wall or mass spectrometer artifacts. The method of $C^{18}O_2$ introduction changed during the study. For catalysts 2, 3, 4, and 5, $C^{18}O_2$ was injected through a septum using a 5- or 10-cc gas syringe (Hamilton Co.) driven by a syringe pump. For catalyst 1, a stainless steel capillary was used to deliver the $C^{18}O_2$ from the lecture bottle. The $C^{18}O_2$ flow rates were chosen to be similar in magnitude to the O_2 used in the catalytic reaction and are listed in Table 1.

Exchange of ethylene oxide was studied by using a similar infusion of natural abundance ethylene oxide (2% in N_2) into the $^{18}O_2$-labelled standard reactant mixture after isotopic equilibrium had been established. This experiment was performed in connection with experiments 2a, 2b, 4, and 5. In these experiments, the EO mixture was introduced into the $^{18}O_2$-containing feed by capillary and

at similar molar flow rates as in the CO_2 exchange experiments. As in the checks of the isotope transient experiments, the isotopic composition of the products in both types of isotope exchange experiments were measured by GCMS.

RESULTS AND DISCUSSION

Reaction Kinetics and Characterization Results

The catalytic activities and selectivities for each of the experiments described in Table 1 are shown in Table 2 along with the post-reaction characterization (XPS and SA) results. The reactant conversions are low enough that the rates can be viewed as differential with respect to reagents; however, even low levels of the CO_2 product have been noted to affect the reaction rates (34–36). The calculated Thiele modulus was 0.03 for the most stringent case (experiment 2b), assuming no internal porosity in the primary silver particles (see below); this indicates that mass transfer rates had no effect on the measured rates. The thermocouple in the catalyst bed registered up to a 3°C temperature rise when the reactants were introduced. The bed was presumed to be isothermal at the measured value, a view supported by simulations.

The reactivities for the various data sets are quite scattered and reflect the wide range of catalyst conditioning and treatments. When normalized to surface area and when direct comparisons can be made (1a versus 1b; 2 versus 3), the chlorine treated catalysts are seen to be less reactive than undosed catalysts. The effects of chlorine aside, the rates are complicated by (minor) changes of the surface area and the characteristics of the resulting surface during the experiments. The low rates for experiment 4 (compare with 1a at a significantly lower temperature) result from the surface annealing and desurfacing caused by the extensive redox treatments at high temperature. Previous investigators have commented on the difficulties in obtaining reproducible surface area specific rates (37, and references therein), even in the absence of chlorine and other "promoters." The initial rates at our standard conditions decayed during the first day or so. No significant changes occurred in the surface areas (see Table 1) of the used catalysts, or in the morphology of the primary particles as a result of pelletization and reaction history, unless the catalyst was exposed to relatively severe conditions (temperatures approaching 300°C and above). In the case of the catalyst from experiment 4, there was a substantial increase in the average particle size and evidence of "necking" between the primary particles as a result of the high temperature redox treatments. The fresh powders gave equivalent surface areas by microscopy and by BET, indicating no internal porosity in the primary particles.

Reaction orders in experiments 1a and 1b were near first order in oxygen (0.6 in 1a and 0.9 in 1b) and near zero order in ethylene (0.03 in 1a and −0.2 in 1b). These values agree with previous studies of unpromoted silver catalysts at our conditions (relatively low partial pressures of the reactants) (4). The reported reaction orders in ethylene tend to increase and oxygen orders decrease as the total pressure increases, but there is much variation in the reported kinetics. For more details, see (4) and references therein.

The ethylene oxide selectivities of the unpromoted catalysts were 30–50%, a range consistent with previous findings

TABLE 2

Kinetics and Characterization Results

Experiment	Temp. [°C]	C_2H_4[a] rate μmol $s^{-1}g^{-1}$	C_2H_4/O_2 conversion	C_2H_4O[b] selectivity	Cl/Ag (XPS)[c]	Surface[d] area (m^2g^{-1})
Fresh	—	—	—	—	0.000	0.12/0.11[e]
1a	227	0.55	0.12/0.22	0.49	—	—
1b	225	0.35	0.08/0.10	0.67	0.042	0.12
Fresh	—	—	—	—	0.000	0.15/0.17[e]
2a	187	0.25	0.06/0.11	0.46	—	—
2b	221	0.76	0.18/0.32	0.49	0.053	0.16
3a	243	0.074	0.02/0.02	0.80	—	—
3b	266	0.118	0.03/0.03	0.81	0.080	0.15
4	285	0.28	0.07/0.15	0.30	0.000	0.08
5	288	0.59	0.08/0.10	0.69	0.073	0.13

[a] Reaction conditions are summarized in Table 1. Feed composition: C_2H_4(0.17)/O_2(0.17)/Ar(0.66).
[b] Carbon atom (or ethylene) basis.
[c] Uncertainties in all XPS ratios = ±0.005.
[d] Surface areas by SEM image analysis for all.
[e] Additional BET for fresh catalyst. SEM images uncertain by ±25%; BET on fresh catalyst ±0.003.

TABLE 3

Summary of Product Oxygen Exchange Experiments

Experiment	Cat. rate[a] C_2H_4O (μmol $s^{-1}g^{-1}$)	Cat. rate[a] CO_2 (μmol $s^{-1}g^{-1}$)	$f^{18}O$, C_2H_4O (GC-MS)	$f^{18}O$, CO_2 (GC-MS)	^{18}O fed (μmol $s^{-1}g^{-1}$)	^{18}O[b] out (μmol $s^{-1}g^{-1}$)
			$C^{18}O_2$ addition to $^{16}O_2$-C_2H_4			
1a	0.27/0.16	0.56/0.24	0.72 ± 0.01	0.57 ± 0.01	1.18	1.27
1b	0.23/0.12	0.23/0.08	0.76 ± 0.02	0.84 ± 0.01	1.48	1.59
2a	0.12/0.06	0.28/0.09	0.93 ± 0.04	0.82 ± 0.01	—	—
2b	0.37/0.28	0.77/0.49	0.45 ± 0.02	0.24 ± 0.02	—	—
3a	0.06/0.05	0.03/0.02	0.71 ± 0.04	0.79 ± 0.02	—	—
3b	0.10/0.08	0.04/0.02	0.63 ± 0.02	0.65 ± 0.03	—	—
4	0.08/0.08	0.39/0.34	0.44 ± 0.04	0.25 ± 0.03	0.50	0.45
5	0.40/0.38	0.38/0.22	0.62 ± 0.02	0.44 ± 0.03	0.98	0.96
			C_2H_4 ^{16}O addition to $^{18}O_2$-C_2H_4			
2a	0.12/—[c]	0.28/—[c]	0.45[d]	>0.95	—	—
2b	0.37/—	0.77/—	—	>0.95	—	—
4	0.08/—	0.39/—	0.40	>0.95	—	—
5	0.40/—	0.38/—	0.60	>0.95	—	—

[a] For all data sets, the initial feed contained C_2H_4(0.17)/$^{16}O_2$(0.17)/Ar(0.59)/Ne(0.07). Ethylene oxide and carbon dioxide catalytic reaction rates are listed as: rate before exchange experiment/rate at steady state during the exchange experiment.

[b] ^{18}O flux out includes only ^{18}O contained in the products (see text).

[c] Only small changes in ^{18}O product rates.

[d] Average over period of ^{16}O ethylene oxide infusion.

under similar conditions (38, 37). A decrease of selectivity on chlorine-free silver with increasing temperature is noted in the literature (2, 8) and is consistent with our results in experiments 1a and 4, although the catalyst from 1a was not analyzed. Chlorine enhances ethylene oxide selectivity by decreasing the combustion rate to a greater extent than the epoxidation rate, resulting in significantly higher ethylene oxide selectivities (67–81%), again consistent with previous studies (14, 15, 39). Two of the samples (2b, 5) showed surface chlorine after the experiments although they were not intentionally dosed. These experiments followed a severe contamination of the flow system and probably were affected by residual chlorine contamination on the walls of the flow system. The selectivities of these catalysts are consistent with the analyzed amount of surface chlorine. The contamination levels in experiments 1a and 2a are unknown since the samples were not removed for analysis after these experiments. The significant change in catalytic performance between 1a and 1b as a result of the intentional chlorine dose indicates much lower (or zero) contamination in 1a. The effects of chlorine are not linear. In one study (14) chlorine coverages less than ~15% of saturation values had little effect on ethylene epoxidation and combustion reaction rates. These inhibition effects are reversible since the reaction mixture slowly removes chlorine from the surface (14, 40, 41). However, on the time scale of a given transient experiment and the associated kinetics characterization, the effect of a chlorine dose was permanent. This method of modifying the catalyst greatly simplified the preparation of the various gas mixtures for the transient experiments.

Oxygen Isotope Exchange Experiments

Table 3 summarizes the conditions and results of the experiments where oxygen exchange between reaction products and the catalyst was investigated.

Ethylene oxide. Upon addition of unlabelled ethylene oxide to $^{18}O_2$–ethylene reactants, the rate of production of ^{18}O-labelled ethylene oxide and CO_2 changed only slightly and by amounts expected by the associated dilution of the reactants. The flow rate of the infused ethylene oxide was uneven in these experiments and average values are presented in Table 3. No detectable ^{16}O appeared in the CO_2 in the reactor effluent during the infusion of ^{16}O-labelled ethylene oxide. Therefore, under typical reaction conditions and residence times here, ethylene oxide does not exchange oxygen with the catalyst and leaves the reactor with the oxygen atom with which it entered (either by feed or reaction). At our conditions, no oxygen from ethylene oxide is transferred to CO_2, either by exchange or by further oxidation of ethylene oxide to carbon dioxide.

Carbon dioxide. The results of the CO_2 exchange experiments are significantly different as shown by the results in Table 3. Figure 1 shows a prompt response in the isotopic

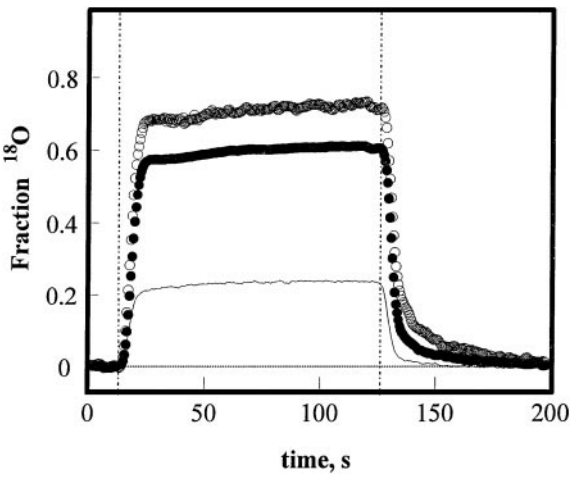

FIG. 1. Appearance of ^{18}O in ethylene oxide (open circles) and CO_2 (solid circles) upon cofeeding of $C^{18}O_2$ (between two vertical dashed lines). Obtained during experiment 1a. See Tables 1, 2, and 3 for reaction conditions. Solid line is the signal for Ne tracer contained in the $C^{18}O_2$ feed.

composition of both products upon sudden introduction of $C^{18}O_2$. Similar results were seen in all such experiments and the results are summarized in Table 3. Several conclusions, some obvious, can be reached from these results.

(1) The oxygen in carbon dioxide is freely exchanged. The ^{18}O in the feed carbon dioxide appears in the carbon dioxide product with close to random (binomial) distribution among the isotopomers $C^{16}O_2$, $C^{16}O^{18}O$, and $C^{18}O_2$. Furthermore, the water product contains ^{18}O. The isotopic composition of water was similar to that in carbon dioxide, but trustworthy measurements were not possible due to mass spectrometer sampling artifacts specifically exchanged with background water on the surfaces of the mass spectrometer vacuum chamber. No such artifacts were associated with the CO_2 measurements. These results agree with previous studies that showed rapid scrambling between carbon dioxide and oxygen-dosed silver under nonsteady state reaction conditions (7, 26–28).

(2) The oxygen in carbon dioxide exchanges with the active oxygen which forms ethylene oxide. The conclusion relies on the appearance of ^{18}O in the ethylene oxide in these experiments and the results of the ethylene oxide experiments above which show that oxygen atoms, once incorporated in ethylene oxide, remain there.

(3) No detectable ^{18}O appears in molecular oxygen under these conditions and residence times. This conclusion is based in part on the direct observation of the ^{18}O content in the molecular oxygen in the effluent, which was indistinguishable from the natural abundance (0.2%). The small uncertainties in these numbers correspond to <5% of the ^{18}O fed with the CO_2 in experiments 1a and 1b. An independent check on this conclusion is obtained by a material balance of ^{18}O in the products. The amount of ^{18}O leaving the reactor (see Table 3) in the products is calculated under the assumption that the water in the product has the same ^{18}O content as carbon dioxide. This amount closely balances the amounts fed to the reactor as $C^{18}O_2$. Oxygen supply to the surface from molecular oxygen is essentially irreversible under these conditions.

(4) The ^{18}O fraction in the two products are not identical. In several of the experiments the ethylene oxide has a somewhat higher ^{18}O content than CO_2 while in others, the situation is reversed. The fact that ethylene oxide in the product does not exchange oxygen once formed means that its isotopic composition is a rate-weighted average over the isotopic composition of the active surface oxygen species in the catalyst bed. Carbon dioxide, on the other hand, continuously adjusts its isotopic composition by exchange so that the products reflects the composition of the catalyst oxygen species at the bed exit.

(5) The catalytic activity for both products decreased during the infusion of carbon dioxide (see Table 3). This effect is in part due to dilution of the reactant gas and in part to product inhibition by carbon dioxide. Carbon dioxide was suppressed more than ethylene oxide, thus producing higher ethylene oxide selectivity. This is generally consistent with previous reports (34–36); however, some researchers have noted that adding carbon dioxide to the feed can also have either no effect or a deleterious effect on ethylene oxide selectivity (26, 42). The dilution effects for experiments 1a and 1b are small because the $C^{18}O_2$ flow rates were small compared to the total gas flow rates (<4%). This is not the case for experiments 4 and 5 because the fraction of the total flow that the $C^{18}O_2$ comprised was much larger (15–20%).

The oxygen flow revealed by the oxygen exchange experiments can be represented by the scheme in Fig. 2. The irreversible flows of oxygen from O_2 to the catalyst and from the catalyst to ethylene oxide are indicated by the unidirectional arrows for these two processes. The exchange of carbon dioxide with one or more pools of surface-bound oxygen is indicated by the two headed arrow and the rapid rate by its width. The catalyst oxygen is represented by a single compartment, but may in fact involve more than one surface intermediate, the identities of which are obscured by post reaction scrambling. This oxygen flow has implications for the isotope transient experiments which are discussed below.

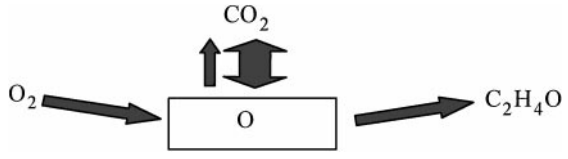

FIG. 2. Diagram of oxygen flow derived from steady state exchange experiments.

Dynamic Isotope Tracing Experiments

Data. Results for the isotope transient $C_2H_4 : {}^{16}O_2 : Ar/Ne \rightarrow C_2H_4 : {}^{18}O_2 : Ar$ are shown for an unpromoted catalyst (experiment 1a in Table 1) in Fig. 3 and for a chlorine inhibited catalyst (experiment 1b) in Fig. 4. The data are plotted as the fraction of ^{16}O in the ethylene oxide and carbon dioxide products as a function of time. The response of the neon tracer in the $^{16}O_2$ stream is also shown; the tail on the tracer washout reflects a short region of laminar flow in the tubing between the switching valve and the catalyst bed. These results typify the entire suite of experiments, which exhibit the following features.

(1) A rapid decay of ^{16}O in the products is seen, initially barely resolved from the tracer and in both cases; this is followed by a slower washout of a remaining portion of the ^{16}O isotope. The initial rapid washout is clearly seen in the inset in Fig. 3. In some experiments, the slow component is very small, as in Fig. 3, and in others, like experiment 1b (Fig. 4), it is a prominent feature. With justification below, we identify the slowly displaced oxygen with the subsurface and the rapid one with surface intermediates.

(2) The slower component in the transients is more pronounced for the chlorided catalyst (1b). This correlation persists in the entire data set and is analyzed quantitatively below.

(3) The oxygen isotopes in the CO_2 product are statistically distributed at every instant throughout the transient. They are thus being rapidly mixed with the participating surface species (including the oxygen which forms ethylene oxide).

(4) The decay curves for ethylene oxide and carbon dioxide products differ slightly in both cases. Such differences persist in all the experiments and are of a similar, relatively small, magnitude. In some cases the differences are almost nonexistent.

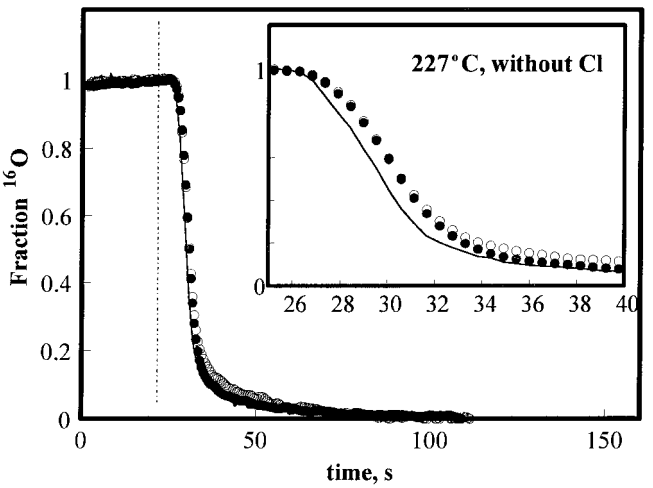

FIG. 3. Steady state $^{16}O_2 \rightarrow {}^{18}O_2$ isotope transient in experiment 1a: Solid circles, ^{16}O fraction in CO_2; open circles, ^{16}O in ethylene oxide; solid line, Ne tracer. $T = 227°C$, no chlorine, $S_{C2H4O} = 0.49$. Inset shows initial phase of transient with greater time resolution.

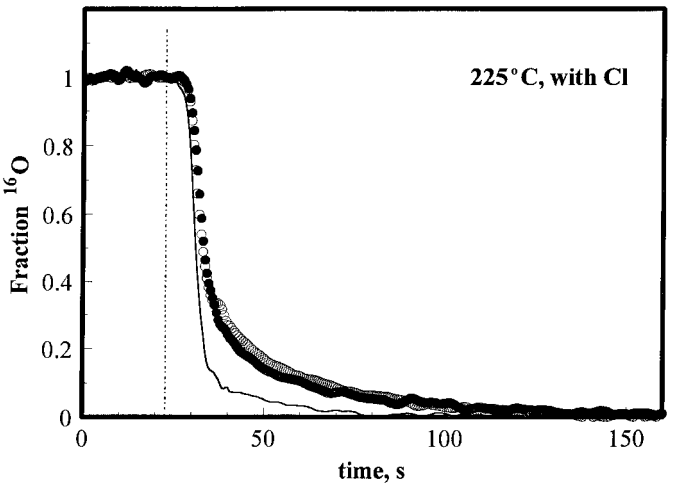

FIG. 4. Steady state $^{16}O_2 \rightarrow {}^{18}O_2$ isotope transient in experiment 1b: Solid circles, ^{16}O fraction in CO_2; open circles, ^{16}O in ethylene oxide; solid line, Ne tracer. $T = 225°C$, chlorine inhibited, $S_{C2H4O} = 0.67$.

Implications of oxygen flow for the isotope transient experiments. An important consequence of the oxygen flow scheme in Fig. 2 is that the isotope washout in the two products is strongly linked during isotope transients. The response curves in the two products are, therefore, similar, and many details regarding the oxygen pathways are obscured. A quantitative analysis of this linkage is not straightforward. As in the steady state tracing experiments above, the ethylene oxide will reflect an average over the dynamically changing catalyst bed during the transient while carbon dioxide reflects the changing composition of the catalyst at the reactor exit. The isotope is transported along the bed by exchange with CO_2 during the transient. This effect, convoluted over the variation over the bed in (1) the amounts of oxygen in the various forms, (2) their connectivity, (3) the reaction rate and (4) selectivity, produces the resulting behaviour. With any of the variations mentioned, the responses in the two products can differ somewhat even if only a single oxygen intermediate exists on the catalyst surface. The remaining subtle differences in the responses may contain further information, but substantial deconvolution of the effects listed above is required to isolate these additional details. We do not undertake this effort here. The gas residence time in the bed is sufficiently short (0.05 s) that it causes little additional convolution of the signal.

Analysis of transient results. The following protocol was used to resolve the number of oxygen intermediates and the pathways of oxygen flow among them. The total amount of active oxygen on the catalyst can be obtained in each case

by simply integrating the total ^{16}O which appears after the tracer. The shape of the washout curve reveals further details about the number of kinetically distinct oxygen intermediates. As reviewed previously (19, 20, 43), the washout response of a reacting system after a sudden isotope switch at reaction steady state can be expressed as a series of decaying exponential terms, some with positive and some with negative coefficients. Each kinetically distinct intermediate is represented by a term in the response. Thus, in the case of a single oxygen intermediate, the response is a single exponential decay

$$f_o(^{16}O) = \exp\{-t/\tau\}.$$

The time constant, τ, is given by

$$\tau = N/r,$$

where N is the amount of the intermediate and r is the rate of its reaction. At least two distinct intermediates are indicated by the complex response in the experimental data. The data for ^{16}O decay for each product in all the experiments were fit to a double exponential decay with the form

$$f_o(^{16}O) = (1-\phi)\exp\{-t/\tau_A\} + \phi\exp\{-t/\tau_B\},$$

where A and B represent the fast and slow components, respectively. Here, f_o denotes the washout curve in the absence of gas residence time effects. Since the isotope switch is not a perfect step function, the inherent product responses must be "deconvolved" from the reactor gas flow behaviour. This was accomplished by an iterative procedure, wherein a nominal analysis was first performed to obtain initial values of the parameters ϕ, τ_A, and τ_B. The experimental results were then simulated by convoluting this initial function over the tracer function to simulate the measured $f(^{16}O)$ and the parameter values adjusted, if necessary, to improve the fit. The final values of the parameters (ϕ, τ_A, and τ_B) are shown in Table 4. The nominal analysis is illustrated in Fig. 5 for the data in experiment 1b. The first step is a "peeling" of the long time constant component from the data (open circles). The tracer function (light solid line) is subtracted from the raw data and the long time tail of the resulting intensity (not shown) is fit by a single

TABLE 4

Summary of Results from $^{16}O_2 \rightarrow {}^{18}O_2$ Dynamic Isotope Tracing Experiments

			Experimental fit[b]			Model parameters[c]							
Experiment[a]	Sel SA	Species	τ_A s	τ_B s	ϕ	N_{tot} μmol/g	θ_{tot}[d] ML	N_1 μmol/g	θ_1 ML	N_2 μmol/g	θ_2 ML	r_{01}	$r_{12}=r_{21}$ μmol g^{-1}s^{-1}
1a	0.49	EO	0.53	18	0.07	0.48	0.22	0.16	0.07	0.32	0.15	0.27	0.019
	0.11	CO_2	0.76	14	0.03	1.82	0.83	1.32	0.60	0.50	0.23	1.69	0.040
		total O	0.75	15	0.04	2.30	1.05	1.48	0.68	0.82	0.37	1.96	0.059
1b	0.67	EO	0.99	31	0.24	1.87	0.85	0.30	0.14	1.57	0.72	0.23	0.066
Cl	0.11	CO_2	1.33	29	0.15	3.78	1.72	1.06	0.48	2.72	1.24	0.68	0.106
		total O	1.26	30	0.17	5.65	2.58	1.36	0.62	4.29	1.96	0.91	0.172
2a	0.46	EO	0.71	22	0.08	0.29	0.09	0.09	0.03	0.20	0.06	0.12	0.010
	0.16	CO_2	0.94	12	0.02	0.98	0.31	0.79	0.25	0.19	0.06	0.82	0.016
		total O	0.90	15	0.03	1.27	0.40	0.88	0.28	0.39	0.12	0.94	0.026
2b	0.49	EO	0.60	41	0.09	1.60	0.50	0.24	0.08	1.36	0.43	0.37	0.036
	0.16	CO_2	0.43	40	0.02	2.86	0.90	1.01	0.32	1.85	0.58	2.32	0.051
		total O	0.48	40	0.03	4.46	1.40	1.25	0.39	3.21	1.01	2.69	0.087
3a	0.8	EO	2.08	34	0.38	0.84	0.28	0.19	0.06	0.65	0.22	0.06	0.030
Cl	0.15	CO_2	1.41	30	0.40	1.14	0.38	0.20	0.07	0.94	0.31	0.09	0.050
		total O	1.60	32	0.39	1.98	0.66	0.39	0.13	1.59	0.53	0.15	0.080
3b	0.81	EO	2.94	32	0.35	1.23	0.41	0.41	0.14	0.82	0.27	0.10	0.037
Cl	0.15	CO2	2.78	26	0.34	1.42	0.48	0.53	0.18	0.89	0.30	0.13	0.048
		total O	2.80	28	0.35	2.65	0.89	0.94	0.31	1.71	0.57	0.23	0.085
5	0.69	EO	0.85	16	0.14	1.29	1.08	0.40	0.33	0.89	0.74	0.41	0.060
Cl	0.06	CO_2	0.25	21	0.06	1.72	1.44	0.31	0.26	1.41	1.18	1.15	0.074
		total O	0.4	19	0.08	3.01	2.52	0.71	0.59	2.30	1.92	1.56	0.134

[a] Experiment numbers as in Table 1. Also included are the ethylene oxide selectivity (C basis) and the surface area from Table 2.

[b] Parameters for double exponential decay fit to oxygen isotope washout: fits to oxygen in ethylene oxide, CO_2 (and H_2O), and the total oxygen flow are included.

[c] Parameters for the compartmental model shown in Fig. 6b obtained from the experimental fits and the relationships in Table 5.

[d] Surface coverages (θ) were calculated from the surface areas assuming a site density of 1.2×10^{19} oxygen atoms/m^2.

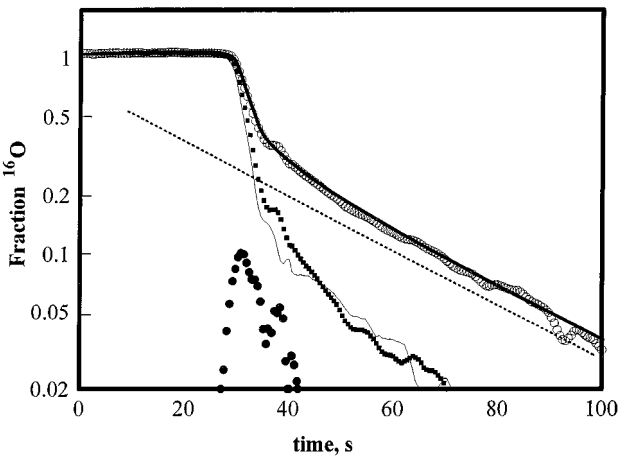

FIG. 5. Processing of ethylene oxide isotope transient data from experiment 1b. Open circles, raw data; thin solid line, tracer. Dashed line, long time, τ_B, component; solid squares, raw data with τ_B component (convoluted over tracer function) subtracted. Solid circles, remainder (τ_A component) after subtracting solid squares from data. Thick solid line, simulation of data by convolution of fit in Table 4 over the tracer function.

exponential (dashed line). The time constant of the exponential is τ_B. The contribution of this component to the transient is given by convoluting this exponential over the tracer function. The area under this convoluted curve is equal to $\tau_B\phi$ (from integration of the equation above), from which the value of ϕ is obtained. The convoluted curve of component B is then subtracted from the raw data, the results are shown as solid squares in Fig. 5. Subtraction of the tracer function from this remaining intensity gives a measure of the contribution of the fast component A. The result (shown by the solid circles) is heavily convoluted over the tracer function. Although the time constant of this portion of the response is not directly resolved, the area associated with this component is. The time constant, τ_A, can therefore be obtained from the fact that this area is given by $(1-\phi)\tau_A$ (again from integration of the equation above). The initial values of ϕ, τ_A, and τ_B are then used to generate f_o, which is convoluted over the tracer function to simulate the experimental data. The solid line through the data in Fig. 5 shows the quality of the fit obtained from these initial values. In each case, very little or no adjustment of the initial values of ϕ, τ_A, and τ_B was required to fit the data well. Clearly, no more than two components can be resolved in the data.

The amounts of oxygen associated with each component represents the seconds of production of the associated product associated with that component of the decay. The amount of oxygen associated with a given component, i, is therefore

$$n_{Ai} = (1-\phi_i)\tau_A v_i r_i : n_{Bi} = \phi_i \tau_B v_i r_i,$$

where v_i is the number of oxygen atoms associated with product i (1 for ethylene oxide and 6 for CO_2 ($+H_2O$)). These values are included in Table 4. The τ_B and ϕ values are similar in the two products during a given experiment—a reflection of the connection between them by exchange. Because of this coupling, the same analysis was performed for the total oxygen flow. The parameters from these analyses, including the total amounts of oxygen, are also included in Table 4.

Compartmental models of the oxygen flow. Two general possibilities exist for the connectivity of the two kinetically distinguishable catalyst oxygen intermediates. These are represented in Fig. 6 by compartmental diagrams where each compartment, or box, represents a kinetically distinguishable intermediate. Using the nomenclature in Ref. (12), the amount of each intermediate is represented by N_i. Each compartment communicates with the gas phase or with other compartments with rates given by

$$r_{ij} = k_{ij} N_j,$$

where the fractional exchange coefficients, k_{ij}, gives the fraction of N_j which flows to i per unit time. The predicted isotope washout curves from both models are double exponential decays and are therefore consistent with the experimental results. Another possible arrangement, with the intermediates connected in series, produces an induction period in the isotope washout that is not evident in the data. One of the models (Fig. 6a) features two "pools" of oxygen in direct contact with the gas phase (and therefore on the catalyst surface) and the other Fig. 6b has only one kinetically distinguishable pool interacting with the gas phase while the other is indirectly connected as a reservoir or "backwater."

The relationships between the parameters in the isotope decay and the parameters for these two models are given in Table 5. These results are derived in Ref. (12). Model (b) gives simplified results (also shown in Table 5) when the two time constants are very different. Model (b), with the indirect coupling of the slow intermediate, is preferred here and we additionally assign pool 1 to surface oxygen

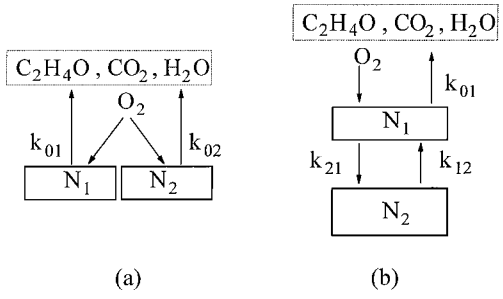

FIG. 6. Models of oxygen flow consistent with isotope transient data: (a) two intermediates reacting in parallel, (b) two intermediates (one direct and one indirect). See text for discussion.

TABLE 5

Relationships between Measured Experimental Parameters and the Compartmental Kinetic Models in Fig. 6

Experimental parameter	In terms of model (a) 2 parallel intermediates	In terms of model (b) 1 direct + 1 indirect intermediate
ϕ	$\frac{N_2 k_{02}}{[N_2 k_{02} + N_1 k_{01}]} = \frac{r_{02}}{(r_{01} + r_{02})}$	$\frac{N_2}{N_1}\frac{(k_{12}\tau_B - 1)}{k_{21}(\tau_A - \tau_B)}$ if $\tau_B \gg \tau_A \approx \frac{k_{12} N_2}{(k_{21} + k_{01}) N_1} = \frac{r_{12}}{(r_{01} + r_{12})}$
τ_A	k_{01}^{-1}	$\frac{2}{[(k_{12} + k_{21} + k_{01})] + [(k_{12} + k_{21} + k_{01})^2 - 4(k_{12} k_{01})]^{0.5}}$ if $\tau_B \gg \tau_A \approx (k_{21} + k_{01})^{-1}$
τ_B	k_{02}^{-1}	$\frac{2}{[(k_{12} + k_{21} + k_{01})] - [(k_{12} + k_{21} + k_{01})^2 - 4(k_{12} k_{01})]^{0.5}}$ if $\tau_B \gg \tau_A \approx k_{12}^{-1}$

and pool 2 to subsurface oxygen. These choices rest on the following considerations.

(1) The rapid exchange with the surface which links the two products implies that the isotopes are rapidly mixed between any chemically distinct surface intermediates, even if their amounts and reactive flow would produce very different lifetimes. A special set of circumstances would be required to have both products show similar decays and extensive isotope exchange, yet retain two pools with distinct lifetimes at the surface. Subsurface oxygen, by being indirectly connected to the gas phase, cannot be homogenized with the surface pool by exchange with the gas.

(2) The absolute amounts of oxygen involved in many cases are more than a monolayer at full coverage, indicating subsurface participation.

(3) Previous non-steady state experiments have shown that subsurface oxygen can form ethylene oxidation products (9).

The amounts of oxygen in the surface and subsurface pools are obtained using the relationships in Table 5 and are presented in Table 4. Because of the large difference in the two lifetimes, the limiting values from the simplified expressions agree with those derived from the full expression to within 5%.

Correlation of results with epoxidation selectivity. We can now make the following observations by comparing the derived values in Table 4 with the catalytic rates and selectivities.

(1) Chlorine increases the available reservoir of subsurface oxygen. This is best appreciated by the direct comparison of the results from experiments 1a and 1b, done sequentially on the same catalyst at the same temperature. The surface oxygen pool appearing in both products (N_1, total) hardly changed upon chlorine addition (1.48 versus 1.36 μmol/g), while the subsurface reservoir (N_2, total) increased from 0.82 to 4.3 μmol/g. Previous TPD experiments (14–17) showed that chlorine increases the amount of subsurface oxygen in silver; the data here show that this effect applies to the steady state reaction.

(2) Chlorine increases the rate of oxygen supply from the long-lived (subsurface) reservoir. The same data show that the rate of supply of O from the subsurface to both products nearly tripled (0.06 to 0.17 μmol $g^{-1}s^{-1}$), while the catalytic rate of oxygen usage decreased by over 50% (1.96 to 0.91 μmol $g^{-1}s^{-1}$). Thus, the increased contribution of subsurface oxygen to the products (shown by increased values of ϕ) is not just a result of a smaller catalytic rate, which allows this flux to compete more effectively, but also from an increased supply rate of subsurface oxygen. This fact could result from an increased oxygen concentration in the bulk or simply a higher mobility which effectively allows oxygen from deeper in the silver to reach the surface in the same time. Measurements of total dissolved oxygen would be instructive here, but were not performed. Mechanistically, chlorine may elevate the surface defect density on silver, which would provide an efficient route for surface oxygen to diffuse from the subsurface (16).

(3) The value of ϕ correlates with the reaction selectivity. Figure 7 shows the ethylene oxide selectivity plotted against ϕ. As ϕ increases, the selectivity increases. The ϕ values for oxygen flow in ethylene oxide are used here, but a similar correlation is obtained if the values for total flow are plotted instead. The regularity is striking, given that the data were obtained on both chlorine-containing and chlorine-free catalysts, over a range of temperatures and with varied pretreatment histories. The data clearly show that larger contributions by subsurface oxygen are associated with higher selectivity. "Prompt" oxygen does not correlate with selectivity.

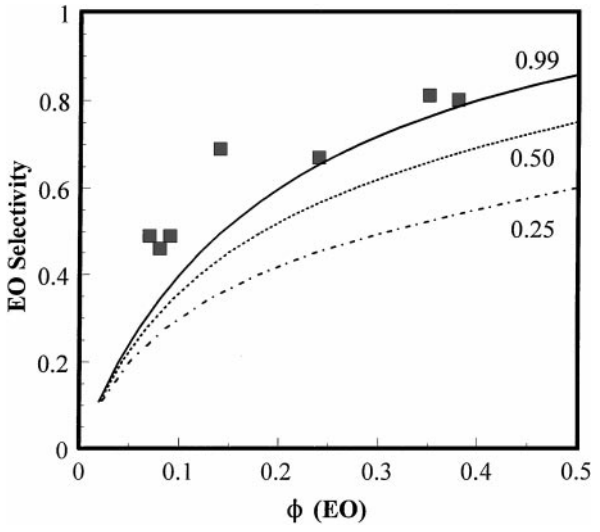

FIG. 7. Correlation between ethylene oxide selectivity and isotope transient parameter ϕ (ethylene oxide). Curves are predictions of simple model described in the text. The curves are labelled with the assumed values of the ratio N_2/N_{tot}.

It is instructive to investigate the quantitative relationship between the oxygen flux from the subsurface and the reaction selectivity. If we assume that the fraction of oxygen that forms ethylene epoxide is equal to the fraction of oxygen that visits the subsurface, the ethylene oxide selectivity (based on oxygen), $S_{\text{EO,O}}$ is given by

$$S_{\text{EO,O}} = r_{12}/(r_{12} + r_{01}).$$

Now, ϕ can be expressed in terms of the exchange coefficients by substitution of the expressions for τ_A and τ_B into the expression for ϕ. Each exchange coefficient can be expressed in terms of $S_{\text{EO,O}}$:

$$k_{01} = (1 - S_{\text{EO,O}})(k_{21} + k_{01})$$
$$k_{21} = S_{\text{EO,O}}(k_{21} + k_{01})$$

and

$$k_{12} = S_{\text{EO,O}} N_1 (k_{21} + k_{01})/N_2.$$

The latter two are obtained from the definition of $S_{\text{EO,O}}$ above and the fact that $r_{12} = r_{21}$. Thus, ϕ can ultimately be expressed as a function of $S_{\text{EO,O}}$ and N_1/N_2,

$$\phi = \frac{S(N+2) - 1 + (1 - 2NS + S^2(N^2 + 4N))^{1/2}}{2(1 - 2NS + S^2(N^2 + 4N))^{1/2}},$$

where $S = S_{\text{EO,O}}$ and $N = N_1/N_2$. Thus, ϕ is not a function only of $S_{\text{EO,O}}$, but it also depends on the partitioning of oxygen between the two pools. Three cases are shown in Fig. 7, each labelled by the fraction of active oxygen in the subsurface pool, f_2 ($f_2 = N_2/(N_1 + N_2)$). The case with the vast majority of oxygen in the subsurface pool ($f_2 = 0.99$) shows a strong resemblance to the experimental data, although the measured values of selectivity are somewhat higher, especially at low values of ϕ. When a smaller fraction of the oxygen resides in the subsurface pool, the selectivity predicted by this model decreases for a given value of ϕ. However, even when the amounts of oxygen in the two reservoirs are equal ($f_2 = 0.5$), the predicted selectivities are still similar to those for $f_2 = 0.99$. If f_2 drops much below this value, however, the predicted selectivities decrease substantially (see the case $f_2 = 0.25$ in the figure). The relative values of τ_A and τ_B are linked to ϕ and f_2. The case where $\tau_B \gg \tau_A$ corresponds to increasingly larger values of f_2 as ϕ increases. In this limit (true for our data), the selectivity predicted by the model is that of the upper limit ($f_2 = 1$) at all values of ϕ.

Selective epoxidation has been previously correlated with a relatively high oxygen inventory in non-steady state experiments (4, 5, 8, 12, 38, 44). The oxygen pumping rate in an electrochemical cell also correlates with epoxidation selectivity (45). This study clearly shows a correlation of epoxidation selectivity with the availability of subsurface oxygen at reaction steady state. The amount of "prompt" surface oxygen, N_1, does not correlate with selectivity. The participation by the subsurface oxygen, particularly its significance in the overall oxygen pathways, is quantitatively linked with increased selectivity. Several explanations are consistent with this fact. One attractive explanation is that the electronic state of the surface oxygen is affected by the presence of subsurface oxygen, making the surface more electrophilic and more selective (6). The connection between our results and such an effect is indirect, since the local oxygen concentration presumably determines the chemical state of the surface. Our measurements yield the flux from the subsurface which is determined by a combination of both the oxygen concentration and mobility. In contrast to this and other "indirect" models, where nonlocal effects are responsible for selectivity changes, are kinetic models in which the reaction selectivity is governed by a dynamic site balance at steady state. For instance, the ability of mobile subsurface oxygen to quickly occupy a site opened by reaction could prevent unselective reactions from occurring in the vicinity of the temporarily exposed metal site. Other models along this line are also possible. The connection between our results and such models are more straightforward, since the probability of "healing" the metal site by subsurface oxygen in this instance is directly related to the flux from the subsurface. The analysis above is consistent with the oxygen from the subsurface being 100% selective, while oxygen that does not sample the subsurface is completely unselective. A better fit to the data could obviously be obtained in an extension of this model, wherein the "prompt" oxygen has a finite epoxidation selectivity. Unfortunately, the results here cannot distinguish among the various scenarios. Even mechanisms that involve distinct surface oxygen reactants for the two products, and

which would predict a different transient behavior for the two products, cannot be distinguished because of the rapid post-reaction exchange. Nevertheless, the agreement with the crude model is striking in view of the simplifying assumptions. Investigations over a wider range of conditions such as at higher pressures where the overall kinetics differ would reveal further insight.

ACKNOWLEDGMENTS

The authors thank the Natural Sciences and Engineering Research Council of Canada (NSERC) for support of this research.

REFERENCES

1. Kilty, P. A., and Sachtler, W. M. H., *Cat. Rev. Sci. Eng.* **10**, 1 (1974).
2. Verykios, X. E., Stein, F. P., and Coughlin, R. W., *Cat. Rev. Sci. Eng.* **22**, 197 (1980).
3. Sachtler, W. M. H., Backx, C., and Van Santen, R. A., *Cat. Rev. Sci. Eng.* **23**, 127 (1981).
4. Van Santen, R. A., and Kuipers, H. P. C. E., *Adv. Catal.* **35**, 265 (1987).
5. Backx, C., Moolhuysen, J., Geenen, P., and van Santen, R. A., *J. Catal.* **72**, 364 (1981).
6. Grant, R. B., and Lambert, R. M., *J. Catal.* **92**, 364 (1985).
7. van Santen, R. A., and de Groot, C. P. M., *J. Catal.* **98**, 530 (1986).
8. Haul, R., and Neubauer, G., *J. Catal.* **105**, 39 (1987).
9. Gleaves, J. T., Sault, A. G., Madix, R. J., and Ebner, J. R., *J. Catal.* **121**, 202 (1990).
10. Grant, R. B., and Lambert, R. M., *Surf. Sci.* **146**, 256 (1984).
11. Backx, C., de Groot, C. P. M., and Biloen, P., *Surf. Sci.* **104**, 300 (1981).
12. Campbell, C. T., and Paffett, M. T., *Surf. Sci.* **143**, 517 (1984).
13. Bukhtiyarov, V. I., Boronin, A. I., Prosvirin, I. P., and Savchenko, V. I., *J. Catal.* **150**, 268 (1994).
14. Campbell, C. T., and Koel, B. E., *J. Catal.* **92**, 272 (1985).
15. Campbell, C. T., *J. Catal.* **99**, 28 (1986).
16. Wu, K., Wang, D., Wei, X., Cao, Y., and Guo, X., *J. Catal.* **140**, 370 (1993).
17. Tan, S. A., Grant, R. B., and Lambert, R. M., *J. Catal.* **100**, 383 (1986).
18. Millar, G. J., Metson, J. B., Bowmaker, G. A., and Cooney, R. P., *J. Chem. Soc. Faraday Trans.* **91**, 4149 (1995).
19. Mims, C. A., Hall, R. B., Jacobson, A. J., Lewandowski, J. T., and Myers, G., *in* "Surface Science of Catalysis: In-Situ Probes and Reaction Kinetics" (F. Hoffman and D. Dwyer, Eds.), ACS Symp. Series 482, p. 230. Amer. Chem. Soc., Washington, 1991.
20. Jacquez, J. A., "Compartmental Analysis in Biology and Medicine," 2nd ed. University of Michigan Press, Ann Arbor, 1985.
21. Shannon, S. L., and Goodwin, J. G., *Chem. Rev.* **95**, 677 (1995).
22. Bulushev, D. A., and Bal'zhinimaev, B. S., *Kinetics Catal.* **37**, 140 (1996).
23. Kim, D. C., *Diss. Abst. Int. B* **53**, 430 (1992).
24. Mauti, R., and Mims, C. A., *Catal. Lett.* **21**, 201 (1993).
25. Jama, A., Master's Thesis, University of Toronto, 1992.
26. Hayes, K. E., *Can. J. Chem.* **38**, 2256 (1960).
27. Keulks, G. W., and Chang, C. C., *J. Phys. Chem.* **74**, 2590 (1970).
28. Bowker, M., Barteau, M. A., and Madix, R. J., *Surf. Sci.* **92**, 528 (1980).
29. Mauti, R., Ph.D. Thesis, University of Toronto, 1994.
30. Czanderna, A. W., *J. Phys. Chem.* **70**, 2120 (1966).
31. Rigas, N. C., Svoboda, G. D., and Gleaves, J. T., ACS Symp. Ser. Vol. 523, p. 183, 1993.
32. Vass, M. I., and Budrugeac, P., *J. Catal.* **64**, 68 (1980).
33. "Handbook of X-Ray Photoelectron Spectroscopy." Perkin-Elmer, Eden Prairie, MN, 1992.
34. Mikami, J., Satoh, S., and Kobayashi, H., *J. Catal.* **18**, 265 (1970).
35. Borman, P. C., and Westerterp, K. R., *Ind. Eng. Chem. Res.* **34**, 49 (1995).
36. Eliyas, A., and Petrov, L., *Appl. Catal.* **62**, 11 (1990).
37. Sajkowski, D. J., and Boudart, M., *Cat. Rev. Sci. Eng.* **29**, 325 (1987).
38. Campbell, C. T., *J. Catal.* **94**, 436 (1985).
39. Yong, Y. S., and Cant, N. W., *Appl. Catal.* **48**, 37 (1989).
40. Ghazali, S., Park, D. W., and Gau, G., *Appl. Catal.* **6**, 195 (1983).
41. Eliyas, A., Petrov, L., and Shopov, D., *Appl. Catal.* **41**, 39 (1988).
42. Stoukides, M., and Vayenas, C. G., *J. Catal.* **69**, 18 (1981).
43. Mirodatos, C., *Catal. Today* **9**, 83 (1991).
44. Akella, L. M., and Lee, H. H., *J. Catal.* **86**, 465 (1984).
45. Karavasilis, Ch., Bebelis, S., and Vayennas, C. G., *J. Catal.* **160**, 190 (1996).